

On a new twist in the dynamics of Bose-Einstein condensation

Boris Nowak and Thomas Gasenzer

*Institut für Theoretische Physik, Ruprecht-Karls-Universität Heidelberg,
Philosophenweg 16, 69120 Heidelberg, Germany and
ExtreMe Matter Institute EMMI, GSI Helmholtzzentrum für
Schwerionenforschung GmbH, Planckstraße 1, 64291 Darmstadt, Germany*
(Dated: March 8, 2013)

The dynamical process of Bose-Einstein (BE) condensation of a dilute ultracold gas is found to occur in two distinctly different forms. If the particle flux into the low-energy modes is sufficiently strong, the Bose gas behaves predominantly like an incompressible fluid. It exhibits chaotic (Vinen) superfluid turbulence which marks the presence of a *non-thermal fixed point* of the evolution. The approach of this state can be identified by the build-up of a characteristic power-law single-particle spectrum $n(k) \sim k^{-5}$. Alternatively, for a weak flux in energy space, during the condensation process phase defects reminiscent of superfluid turbulence appear but a separation of the incompressible and compressible components, as well as the k^{-5} scaling of the low-energy modes are absent.

PACS numbers: 11.10.Wx 03.75.Lm 47.27.E- 67.85.De

Introduction. In view of the rapid progress in experimental control of Bose-Einstein condensates (BEC) in dilute atomic gases, a growing community is investigating the nonequilibrium dynamics of these systems. One of the most fundamental and long debated questions concerns the formation of a BEC from a completely disordered initial state [1–20]. A particularly interesting aspect is the role of superfluid turbulence in this process [3–5, 14, 16]. Understanding the possible different paths to a BEC is of fundamental interest way beyond the realm of ultracold gases, from the phenomenology of the solid state up to the highest energies, e.g., in heavy-ion collisions [21–25] or early-universe evolution [21, 26–29].

Bose-Einstein condensation in a non-equilibrated and under-cooled gas can have the characteristics of a turbulent inverse cascade [3, 4, 14], corresponding to a quasi-local transport process in *momentum* space, into the low-energy modes of the Bose field. At energies below the regime where this cascade is expected to be described by kinetic weak-wave-turbulence theory [3, 4], a period with superfluid turbulence can appear which manifests itself through the appearance of vortex tangles [5, 14].

In this article, we demonstrate that the superfluid turbulence period can appear in two distinctly different forms. Suppose we start with a dilute, incoherent homogeneous gas in three dimensions, at a temperature close to and above the BEC phase transition. Apply a cooling quench by removing particles from the higher-energy modes. After this, the system re-equilibrates to thermal equilibrium, with a temperature given by the total energy of the system after the quench which we assume to be below the BEC critical temperature.

Two different scenarios are possible: If a sufficiently small amount of energy is removed, the induced scattering of particles into the low-energy modes builds up a thermal Rayleigh-Jeans distribution in a quasi-adiabatic way. The chemical potential increases, and a fraction of particles is deposited in the lowest mode, forming a

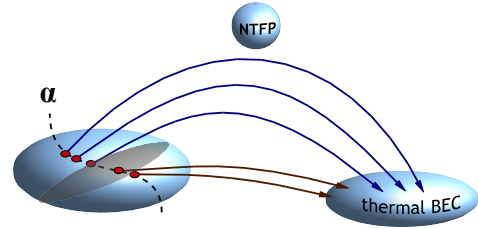


FIG. 1: (Color online) Depending on the strength α of an initial cooling quench, the gas can thermalize directly to a Bose-Einstein condensate, or it can first approach and critically slow down near a non-thermal fixed point (NTFP). There it is characterized by a self-similar particle spectrum $n(k) \sim k^{-5}$ and strong Vinen superfluid turbulence.

BEC. During this process, tangles of defect lines can be found in the Bose field by filtering out short-wavelength fluctuations [14]. While the field has a phase winding around these defects, the flow pattern in their vicinity is distorted by strong phase fluctuations.

In the second scenario, after a sufficiently strong cooling quench, the resulting super-thermal population of the higher-energy modes results in a vigorous transport towards lower energies that has the form of a strong-wave-turbulence inverse cascade. This cascade induces a long-lived, power-law single-particle spectrum $n(k) \sim k^{-\zeta}$, with an exponent $\zeta = 5$ distinctly larger than the exponent $\zeta = 2$ which characterizes a thermal Rayleigh-Jeans distribution. The emergence of the strong cascade can be explained by the dominance of incompressible, transverse, vortical superfluid flow over compressible, longitudinal sound excitations and density fluctuations in the respective regime of wave lengths. The power law k^{-5} is traced back to the flow pattern around the vortex lines [33] in the Vinen tangles [30] which become visible without filtering out short-wavelength fluctuations. The possibility of a strong cascade was pointed out in Refs. [27, 28, 31], where this quasi-stationary scaling solu-

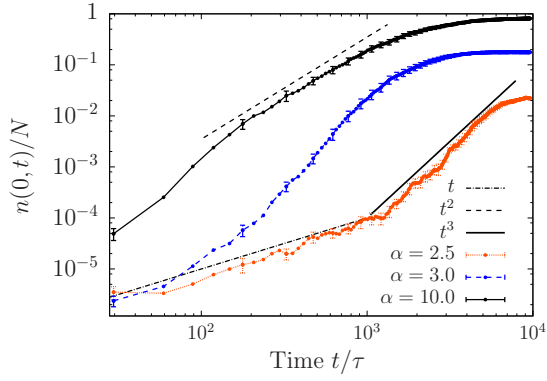


FIG. 2: (Color online) Build-up of the condensate fraction $n(\mathbf{k} = 0, t)/N$ on a double-logarithmic scale, for different strengths of the initial cooling quench, parametrized by the exponent α , cf. Eq. (2). Depending on α , different power-law behavior is seen. Standard averaging errors are shown.

tion was referred to as a non-thermal fixed point (NTFP). The two possible paths to BE condensation are shown schematically in Fig. 1. Whether the system, during the condensation dynamics, can approach the NTFP where the process critically slows down, or whether it moves in a direct way to thermal equilibrium depends on the initial conditions, i.e., on the strength of the cooling quench. We refer to the condensation process which takes the ‘detour’ via the NTFP as *hydrodynamic BE condensation* because of the dynamical separation of incompressible and compressible components in momentum space, in contrast to the direct process where this separation is absent.

Semiclassical simulations. To reveal this dynamics we study a dilute Bose gas, in the classical-wave limit, using the Gross-Pitaevskii equation (GPE) ($\hbar = 1$)

$$i\partial_t \phi(\mathbf{x}, t) = \left[-\frac{\nabla^2}{2m} + g|\phi(\mathbf{x}, t)|^2 \right] \phi(\mathbf{x}, t). \quad (1)$$

We consider a gas of N atoms in a box of size L^3 , with periodic boundary conditions and mean density $\bar{n} = N/L^3$. We measure length in units of the healing length $\xi = (2mg\bar{n})^{-1/2}$ and time in units of $\tau = m\xi^2$. Simulations were done on a cubic grid with 256^3 points.

The initial field in momentum space, $\phi(\mathbf{k}, 0) = \sqrt{n(\mathbf{k}, 0)} \exp\{i\varphi(\mathbf{k}, 0)\}$, is parametrized in terms of a randomly chosen phase $\varphi(\mathbf{k}, 0) \in [0, 2\pi)$ and a density $n(\mathbf{k}, 0) = f(k)\nu_{\mathbf{k}}$, with $\nu_{\mathbf{k}} \geq 0$ drawn from an exponential distribution $P(\nu_{\mathbf{k}}) = \exp(-\nu_{\mathbf{k}})$ for each \mathbf{k} . We choose the structure function

$$f(k) = \frac{f_\alpha}{k_0^\alpha + k^\alpha}, \quad (2)$$

for different values of α , with cutoff $(k_0\xi)^\alpha = 0.2/0.44^\alpha$ and normalization $f_\alpha = 400/0.44^\alpha$. We compare results for a range of different cooling quenches defined by the power-laws $\alpha = 2.5, \dots, 10.0$, varying the total number between $N = 10^9$ ($\alpha = 2.5$) and $N = 4.3 \times 10^8$ ($\alpha = 10$).

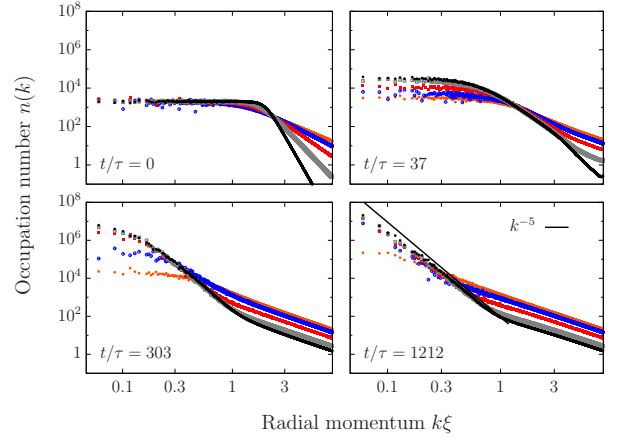


FIG. 3: (Color online) Particle momentum spectra at four different times, on a double-logarithmic scale as functions of the radial momentum $k = |\mathbf{k}|$ for different $\alpha = 2.5$ (orange), 3.0 (blue), 4.0 (red), 6.0 (grey), 10 (black), from top to bottom at $k\xi = 1$. Averages over 3..7 runs. A steep infrared power-law $n(k) \sim k^{-5}$ appears for $\alpha > 3$.

Evolution of the zero mode. The initial power-law fall-off of $f(k)$ chosen above is close to or steeper than that expected by a self-similar solution of the wave Boltzmann equation, $\alpha \simeq 2.4$ [7], corresponding to an inverse particle cascade in weak wave turbulence theory [3, 4]. $\alpha = 2$ would correspond to a stable initial thermal distribution at finite chemical potential, and thus any $\alpha > 2$ is required to set off a re-equilibration to a lower temperature. In Fig. 2 we show the ensuing time evolution of the condensate occupation number $n(0, t)$ for the different α . In each case, the evolution leads to a BEC characterized by a non-vanishing ratio $n(0, t)/N$. As we keep f_α and k_0^α constant $n(0, t)/N$ grows with α . This is because larger α cut off more high-momentum particles and leave less energy to be thermally redistributed. Power-law growth $n(0, t) \sim t$ [3], $\sim t^3$ [6], and $\sim t^2$ is seen.

Momentum distribution. Beyond the zero mode, the occupation spectrum of the non-zero momentum modes allows to follow the dynamical process of potentially turbulent particle transport to lower energies. In Fig. 3 we show the time evolution of the single-particle distribution $n(k, t)$ over the radial momenta $k = |\mathbf{k}|$ at four different times and for the different α . During the initial evolution ($t \lesssim 10^2\tau$) the mode occupations gradually spread to lower wave numbers, at the same time depositing energy into the high-momentum tail. Our dynamic range does not allow to identify a weak-turbulence inverse particle cascade with $n(k) \sim k^{-2.4}$ [7]. At late times, the spectra developing from the different initial α differ strongly. For $\alpha \gtrsim 3$, the distribution develops a bimodal structure, with a power-law behavior $n(k) \sim k^{-5}$ in the infrared (IR) and $n(k) \sim k^{-2}$ in the UV. At very long times, this bimodal structure decays towards a global $n(k) \sim k^{-2}$ (not shown). For $\alpha \lesssim 3$, the distribution directly reaches

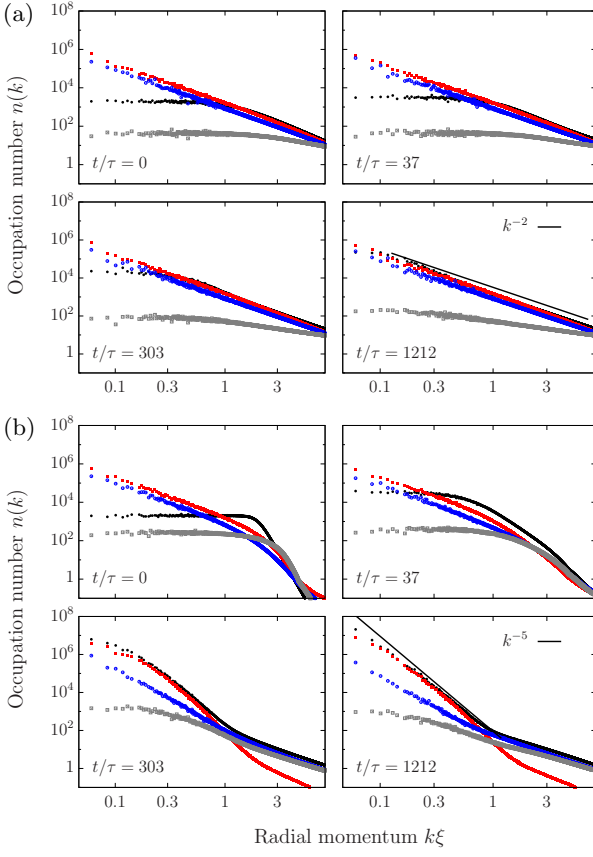


FIG. 4: (Color online) Decomposition of particle spectra $n(k)$ (black) into incompressible (red), compressible (blue), and ‘quantum-pressure’ (grey) components, see text for definitions, on a double-log scale, at four different times. (a) Weak cooling quench, $\alpha = 2.5$. Average of 3 runs (b) Strong quench, $\alpha = 10$. Average of 7 runs

a thermal Rayleigh-Jeans scaling $n(k) \sim T/k^2$. We point out that the strongly nonthermal k^{-5} power law was recently predicted in a non-perturbative quantum-field-theory approach to strong wave turbulence [21, 31]. Its origin has been related to the presence of a dilute gas of vortices [32, 33].

Hydrodynamic condensation. To interpret our results in the context of superfluid turbulence we analyse kinetic-energy spectra as in [34]. The kinetic energy $E_{\text{kin}} = \int d\mathbf{x} \langle |\nabla\phi(\mathbf{x}, t)|^2 \rangle / 2$ is split, $E_{\text{kin}} = E_v + E_q$, into the ‘classical’ component $E_v = \int d\mathbf{x} \langle |\sqrt{n}\mathbf{v}|^2 \rangle / 2$ with velocity $\mathbf{v} = \nabla\phi/m$, and a ‘quantum-pressure’ component $E_q = \int d\mathbf{x} \langle |\nabla\sqrt{n}|^2 \rangle / 2$. Radial particle spectra

$$n_\delta(k) = \frac{1}{2} \int d\Omega \langle |\mathbf{w}_\delta(\mathbf{k})|^2 \rangle, \quad \delta = v, q. \quad (3)$$

in terms of the generalised velocities $\mathbf{w}_v = \sqrt{n}\mathbf{v}$ and $\mathbf{w}_q = \nabla\sqrt{n}$ are furthermore decomposed by $\mathbf{w}_v = \mathbf{w}_i + \mathbf{w}_c$ into ‘incompressible’ ($\nabla \cdot \mathbf{w}_i = 0$) and ‘compressible’ ($\nabla \times \mathbf{w}_c = 0$) parts to distinguish vortical superfluid and sound excitations of the gas, respectively. In Fig. 4a,

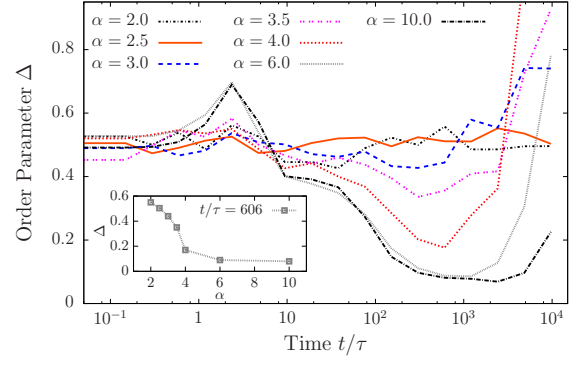


FIG. 5: (Color online) Evolution of the fraction Δ of integrated compressible to incompressible components below a momentum scale $k\lambda\xi = 0.35$, for different initial conditions. Note the semi-log scale. For $\alpha \lesssim 4$, $\Delta(t)$ stays approximately constant. For $\alpha \gtrsim 4$, $\Delta(t)$ approaches zero at intermediate times, signaling the non-thermal fixed point and a superfluid hydrodynamic condensation process. Averages over 1...7 runs. Inset: $\Delta(t = 606\tau)$ as a function of α .

we show the evolution of the different components $n_\delta(k)$, $\delta \in \{i, c, q\}$, for the weak initial quench $\alpha = 2.5$. At early times, $t \lesssim 10^3\tau$, due to the absence of phase coherence [33] the resulting spectra do not add up to the single-particle spectrum $n(k) \neq n_i(k) + n_c(k) + n_q(k)$. Compressible and incompressible components are roughly of equal magnitude while the quantum pressure component is insignificant on all scales. $n(k)$ grows in the regime of low momenta while phase coherence is being established and a condensate fraction appears (Fig. 2). For the case of the strongly non-thermal initial distribution, $\alpha = 10$, the evolution is shown in Fig. 4b. In contrast to Fig. 4a, two macroscopic flows can be observed, one to the UV, and one to the IR. Conservation of particle and energy imply immediately that, when sent out from the regime of intermediate frequencies, energy is deposited in the UV while particles are predominantly transferred to the IR. This leads to an inverse particle cascade with approximately k -independent radial particle flux $Q(k) \equiv Q$ and a corresponding direct energy cascade to the UV [33]. The inverse particle cascade reflects strong wave turbulence, characterized by $n(k) \sim k^{-5}$ [31]. The decomposition in Fig. 4a makes clear that this power-law is caused by incompressible excitations only [32, 33], establishing a dominantly ideal *hydrodynamic* (superfluid) BE condensation process. In the UV, the excitations follow a thermal $n(k) \sim k^{-2}$ and are dominated by the compressible and quantum-pressure components.

Our results show that during the hydrodynamic condensation process incompressible flow temporally dominates at the expense of compressible excitations in the IR regime. The opposite occurs for the compressible excitations in the UV. This dynamical separation marks the approach to the NTFP and disappears when the system finally approaches thermal equilibrium. The evolution of

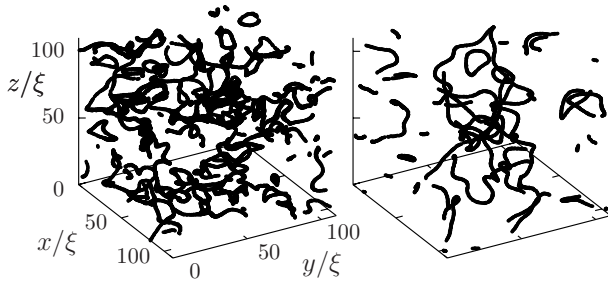


FIG. 6: (Color online) Vortex tangle structures emerging in the gas for the two different extremes of initial conditions, $\alpha = 2.5$, at time $t = 2424\tau$ (left) and $\alpha = 10$, at time $t = 606\tau$ (right).

the integrated fraction $\Delta(t) = N_c(k_\lambda, t)/N_i(k_\lambda, t)$, with $N_\delta(k_\lambda, t) = \int_{|\mathbf{k}| < k_\lambda} d\mathbf{k} n_\delta(\mathbf{k}, t)$, of compressible to incompressible occupations below a momentum scale $k_\lambda \xi = 0.35$ is shown in Fig. 5. Initially, $\Delta \sim 0.5$. Starting from $\alpha \leq 3$, Δ stays approximately constant while for $\alpha > 3$, Δ decreases for $t \gtrsim 10^2\tau$ towards zero before increasing again when thermal equilibrium is approached. The inset shows $\Delta(t = 606)$ as a function of α in which one identifies a transition to a separation of the components, depending on the strength of the initial cooling quench.

Defect formation. In Fig. 6 we show the three dimensional distribution of points where the density falls below 0.2% of the average density \bar{n} , for the systems quenched with $\alpha = 2.5$ and $\alpha = 10$, at the times $t = 2424\tau$ and 606τ , respectively. We filtered out modes with wavenumber larger than $k\xi = 0.45$ but in the hydrodynamic case the high-momentum fluctuations barely distort the figure. The vortex tangles corroborate the findings of [14] for both cases of α . However, a remarkable difference exists in the distribution of the phase angle $\varphi(\mathbf{x})$ of the Bose field as can be inferred from Fig. 4. While in the direct condensation case, the circular flow has strong longitudinal (compressible) fluctuations, in the hydrodynamic condensation via the NTFP macroscopic quantized vortical flow and thus Vinen turbulence of the superfluid are built up. Fig. 2 indicates a change in the power-law rise $n(0, t) \sim t^\nu$ from $\nu \sim 3$ to $\nu \sim 2$ to be associated with the approach of the NTFP. Similar features have been found to characterize the dynamics of a two-dimensional superfluid near a NTFP [35].

Summary. We find Bose-Einstein condensation in a dilute ultracold gas to occur in two different forms. Hydrodynamic condensation involves a distinct dominance of incompressible flow bearing chaotic (Vinen) turbulence, corresponding to an approach of a *non-thermal fixed point*. In this regime, particles can not be deposited quickly enough into the zero mode and form an excess population with a characteristic power-law fall-off within the low-energy modes. In contrast, direct condensation can exhibit the appearance of vortical motion but lacks

its separation from compressible sound-like excitations. The found characteristic power-law growth of the condensate fraction allows to distinguish the regimes in experiment.

Acknowledgements. We thank N. Berloff, J. Berges, J. P. Blaizot, S. Erne, M. Karl, L. McLerran, N. Philipp, J. Schole, D. Sexty, and B. Svistunov for useful discussions. Work supported by Deutsche Forschungsgemeinschaft (GA677/7,8), University of Heidelberg (FRONTIER), and Helmholtz Association (HA216/EMMI).

-
- [1] E. Levich and V. Yakhot, Phys. Rev. B **15**, 243 (1977); J. Phys. A: Math. Gen. **11**, 2237 (1978).
 - [2] H. T. C. Stoof, Phys. Rev. Lett. **66**, 3148 (1991).
 - [3] B. Svistunov, J. Mosc. Phys. Soc. **1**, 373 (1991).
 - [4] Y. Kagan, B. V. Svistunov, and G. V. Shlyapnikov, [Zh. Eksp. Teor. Fiz. 101, 528 (1992)] Sov. Phys. JETP **74**, 279 (1992).
 - [5] Y. Kagan and B. V. Svistunov, [Zh. Eksp. Teor. Fiz. 105, 353 (1994)] Sov. Phys. JETP **78**, 187 (1994).
 - [6] K. Damle, S. Majumdar, and S. Sachdev, Phys. Rev. A **54**, 5037 (1996).
 - [7] D. Semikoz and I. Tkachev, Phys. Rev. D **55**, 489 (1997).
 - [8] Y. Kagan and B. V. Svistunov, Phys. Rev. Lett. **79**, 3331 (1997).
 - [9] D. Snoke and J. Wolfe, Phys. Rev. B **39**, 4030 (1989).
 - [10] C. W. Gardiner, M. D. Lee, R. J. Ballagh, M. J. Davis, and P. Zoller, Phys. Rev. Lett. **81**, 5266 (1998).
 - [11] H. Miesner, et al., Science **279**, 1005 (1998).
 - [12] P. Drummond and J. Corney, Phys. Rev. A **60**, 2661 (1999).
 - [13] M. Köhl, et al., Phys. Rev. Lett. **88**, 080402 (2002).
 - [14] N. G. Berloff and B. V. Svistunov, Phys. Rev. A **66**, 013603 (2002).
 - [15] C. Connaughton, et al., Phys. Rev. Lett. **95**, 263901 (2005).
 - [16] S. Nazarenko and M. Onorato, Physica D: Nonlin. Phen. **219**, 1 (2006).
 - [17] S. Ritter, et al., Phys. Rev. Lett. **98**, 090402 (2007).
 - [18] C. N. Weiler, et al., Nature **455**, 948 (2008).
 - [19] E. V. Kozik and B. V. Svistunov, J. Low Temp. Phys. **156**, 215 (2009).
 - [20] R. P. Smith, et al., arXiv: 1112.4457 [cond-mat.quant-gas] (2011).
 - [21] J. Berges, S. Scheffler, and D. Sexty, Phys. Lett. **B681**, 362 (2009).
 - [22] M. Carrington and A. Rebhan, Eur. Phys. J. **C71**, 1787 (2011).
 - [23] K. Fukushima and F. Gelis, Nucl. Phys. **A874**, 108 (2012).
 - [24] J.-P. Blaizot, et al., Nucl. Phys. **A873**, 68 (2012).
 - [25] J. Berges and D. Sexty, Phys. Rev. Lett. **108**, 161601 (2012).
 - [26] R. Micha and I. I. Tkachev, Phys. Rev. Lett. **90**, 121301 (2003).
 - [27] J. Berges, A. Rothkopf, and J. Schmidt, Phys. Rev. Lett. **101**, 041603 (2008).
 - [28] J. Berges and G. Hoffmeister, Nucl. Phys. **B813**, 383 (2009).

- [29] T. Gasenzer, B. Nowak, and D. Sexty, Phys. Lett. **B710**, 500 (2012).
- [30] G. E. Volovik, J. Low Temp. Phys. **136**, 309 (2004).
- [31] C. Scheppach, J. Berges, and T. Gasenzer, Phys. Rev. A **81**, 033611 (2010).
- [32] B. Nowak, D. Sexty, and T. Gasenzer, Phys. Rev. B **84**, 020506(R) (2011).
- [33] B. Nowak, J. Schole, D. Sexty, and T. Gasenzer, Phys. Rev. A **85**, 043627 (2012).
- [34] C. Nore, M. Abid, and M. E. Brachet, Phys. Rev. Lett. **78**, 3896 (1997).
- [35] J. Schole, B. Nowak, and T. Gasenzer, arXiv: 1204.2487 [cond-mat.quant-gas] (2012).